Two-slope Path Loss Model for Curved-Tunnel Environment with Concept of Break Point

Kalyankar Shravan Kumar*, Yee Hui Lee*, and Yu Song Meng†
School of Electrical and Electronic Engineering, Nanyang Technological University (NTU), Singapore
†National Metrology Centre, Agency for Science, Technology and Research (A*STAR), Singapore

***Abstract*—The curvature of tunnels introduces an extra loss in the wave propagation. A simulation and measurement study are performed on the straight and the curved tunnels to investigate the extra loss in the curved tunnels in comparison with the straight tunnels at a frequency of 2.4 GHz. This study suggests the existence of two wave propagation mechanisms in the curved tunnel; *enhanced waveguiding mechanism* induced by rich multipath components from the curved tunnels and *degraded waveguiding mechanism* due to the blockage from the curved tunnel walls. For efficient radio planning, a new propagation model with curvature dependent break point is proposed. The proposed break point indicates the end of the *enhanced waveguiding mechanism* and the beginning of the *degraded waveguiding mechanism*. A two-slope radio wave propagation model is then proposed for radio communications inside curved tunnels by using the determined break point, with performance evaluation.**

***Index Terms*—Channel models, tunnel propagation, path loss measurement, curved tunnel, two-slope model, waveguiding effect.**

I. INTRODUCTION

The current railway industry is facing three challenges; to increase capacity, to lower costs and to improve customer satisfaction. Communications-Based Train Control (CBTC) is a promising railway technology that can address these challenges by providing an accurate location of the train and reduce the time interval between the trains. The benefits of CBTC can be achieved by providing a reliable radio communication along the rail route. Nearly all the CBTC systems around the world use ISM band frequencies for train signaling. Among the 900 MHz, 2.4 GHz and 5.8 GHz in the ISM band, 2.4 GHz frequency band is most widely used because of availability of large vendor market and industrial support for the radio equipment [1]. The train communication can be established by using leaky cables, discrete antenna and free space optical (FSO) communication system [2]–[4]. It should be noted that the current progress in technology to 5G systems for example for sub-7GHz is in the range for 3.5 GHz in Singapore. Therefore, the results presented here are applicable and will be applicable for future system upgrading. The discrete antenna-based communication system is often used because it is less expensive and easier to install [2]. The tunnels are recognized as one of the most complex radio propagation environment with rich multipath propagation [1], [5].

Proper modeling of radio wave propagation in a tunnel environment plays a crucial role in deploying Access Points and is essential for the installation of radio communication systems. The developed channel models can help in determining the number and position of base stations, and also allowing for the radio system optimization. The waveguide-like structure of tunnels and the electrical properties of tunnel walls have motivated many researchers to develop a waveguide-based channel model for mines and railway tunnels [6], [7]. It is noted that the attenuation rate in tunnels is much lower than that of free space and will decrease when the operating frequency increases. This unique feature of tunnels can be utilized to improve radio communications in tunnels through developing proper channel models and thereby reducing network infrastructure costs.

In the literature, Mahmoud and Wait [8] proposed a waveguide-based channel model for tunnel propagation and discussed the characteristics of multimode propagation. The received signal in the tunnels is a result of the combination of different order modes. The analytical expressions for calculating the received signal power along the tunnel are presented by Sun and Akyildiz [9].

In addition, ray tracing is also popular in studying the propagation of radio waves in the tunnel environments. Several channel modeling approaches were proposed based on ray tracing techniques [10]–[12]. The ray tracing tools represent a possible satisfactory solution in theory, but in practice their actual reliability strongly depends on the accuracy of the environment description and the available computational capacity [6], [12].

From the literature, empirical models can provide better accuracy, although they are site-specific and require heavy manpower resources for model developments. Over the years, researchers have been working on the understanding of key parameters which can affect the radio wave propagation in tunnels by performing extensive channel soundings and measurements.

The electromagnetic field distribution along the tunnel is sensitive to the position of a transmitter antenna and the radio wave polarization. The optimal polarization of the transmitted radio wave should be decided by considering the cross-section and the geometry of the tunnels. For wide but low tunnels, the horizontally polarized wave experiences much lower attenuation than the vertically polarized wave, and vice versa [13]. Placing the transmitter antenna with suitable polarization at the optimal location will reduce the propagation loss. The middle of the tunnel is considered as the optimal location for both vertical polarization and horizontal polarization, and the field distribution has the least effect of strong reflected signals from sidewalls compared to other locations inside the tunnel [14]. However, placing the transmitter antenna in the middle of the tunnel is impractical in many cases. The antenna should be placed at the location where the antenna radiations are least blocked by the tunnel walls. In case of vertical polarization,

the optimal antenna position is at the upper middle of the wall, while for horizontal polarization, the optimal position is in the middle of the sidewall [14]. It is also reported that the effect of humidity on the electrical parameters of the tunnels is negligible, and the conductivity and permittivity of tunnel walls can be treated as a constant [15] [16].

Moreover, it is found that most of the tunnel propagation models were developed for a straight tunnel that cannot be used for a curved tunnel directly since the curvature of the tunnel can introduce extra attenuation/loss [17] which may cause unexpected breakdown of communication links. Therefore, in this paper, we attempt to accurately determine the distance from the transmitter in a curved tunnel at which the tunnel will start to introduce extra loss. We have proposed a new approach to calculate this distance by using the antenna position and the radius of curvature (ROC) of the tunnel. This distance can be treated as the break point between *the enhanced waveguiding mechanism* and *the degraded waveguiding mechanism* which will be discussed later. A two-slope propagation loss model is then proposed to address the curved-tunnel radio wave propagation.

In the rest of the paper, Section II presents a review and summary of those experimental works and empirical models published in the literature. In Section III, the measurement site, setup, and methodology are described. Comparison study of the straight-tunnel and the curved-tunnel radio wave propagation is reported in Section IV. The proposed method for break point calculation and the justification for the existence of both the enhanced and degraded waveguiding mechanisms are given in Section V, where a two-slope propagation loss model is proposed for curved tunnels. Finally, the concluding remarks are drawn in Section VI.

II. Review on Empirical Propagation Models in Tunnels

A. Empirical Models for Straight Tunnels

Many empirical models were proposed in the literature to predict radio wave propagation in tunnels. The two-slope model is the most popular approach which separates the propagation regions into the near zone and the far zone [18], [19]. The region adjacent to the transmitter antenna where the first Fresnel zone is not wide enough to reach any of the tunnel walls is considered as the near zone. The effect of the reflected and diffracted signals is negligible in the near zone. The far zone is the region where the reflected and diffracted signals have a significant impact on the received signal. It is noted that the near-zone propagation can be approximated by a free space channel and the far-zone propagation can be approximated by a waveguiding channel (e.g., presented as the waveguide model). Recently a four-slope model [20]–[22] was introduced by dividing the propagation regions in sequence further as free space propagation, multimode propagation, fundamental-mode propagation, and free space propagation. The detailed propagation mechanisms along the tunnel are determined based on the dimensions of the tunnel and the wavelength of the radio signal. In [23] a five-zone propagation model was also proposed to consider the impact of large-sized vehicles inside the tunnel. The region close to the transmitting antenna in the presence of a large-sized vehicle can be considered as a near shadowing zone. However, it is observed that most of the reported models were developed to address the challenges in straight tunnels which may not be applicable to a curved tunnel.

B. Empirical Models for Curved Tunnels

Measurements have been carried out to study the effects of cross-section, operating frequency, polarization and ROC on radio wave propagation in tunnels [13], [17]. Both the studies concluded that curved tunnels can reduce the waveguiding effect, and hence the propagation loss in curved tunnels are higher than that in straight tunnels. Moreover, an extra loss introduced by the tunnel curvature was reported to be directly proportional to the ROC. When the operating frequency increases, the waveguiding effect will increase but this extra loss introduced by the tunnel curvature can nullify it.

In [17], a study on polarization shows that horizontally polarized wave propagation is influenced by the change in reflection coefficients on the sidewalls of the tunnel, while the vertically polarized wave propagation is mainly influenced by the reflected signals from the roof and floor of the tunnels. The horizontally polarized wave experiences relatively higher attenuation from tunnel curvature, compared with vertical polarization. Since most of the tunnels include straight and curved segments, vertically polarized wave is preferred due to its lower attenuation rate as compared to that of the horizontally polarized wave.

In their studies, it is concluded that the extra loss due to the tunnels curvature can range from $(0.8 - 6.7)$ dB/100 m [17] which varies with the dimensions of the tunnel and the ROC. This extra loss is reported to be consistent for all the frequencies within the ISM band in [13]. By adding the value of extra loss (EL_{curve}, in dB/100 m) to the straight tunnel path loss $L_{straight}$ in dB, a curved-tunnel path loss L_{curved} in dB can be determined as

$$L_{curved} = L_{straight} + EL_{curve} \cdot \left(\frac{d(m)}{100\ m} \right) \qquad (1)$$

However, the location from which the extra loss shall be considered has not been addressed.

This motivates us to perform an in-deep study to investigate in detail those different radio wave propagation mechanisms in a curved tunnel through a comparative study with a straight tunnel. The extra loss in curved tunnels is found to be caused by the degraded waveguiding mechanism. A break-point model is therefore proposed to calculate the point within the curved tunnel at which the waveguiding effect starts to degrade. By using the proposed break point, a two-slope model is developed to predict the propagation loss by considering *the enhanced waveguiding mechanism* and *the degraded waveguiding mechanism* in curved tunnels. Details will be discussed below.

III. Measurement Methodology

A. Tunnel Under Investigation

The measurements were performed along arched subway tunnels in Singapore. The tunnel segment has a modern arch-

shaped structure with a maximum width of 5.8 m and a radius of 2.9 m. The distance from the floor to the center of the arch is 1.6 m as illustrated in Fig. 1. These tunnels have a pathway along the track for maintenance workers. Additionally, these tunnels are made of concrete and consist of rail tracks, pipes, cables and some metallic objects which can introduce multiple reflection and scatterings.

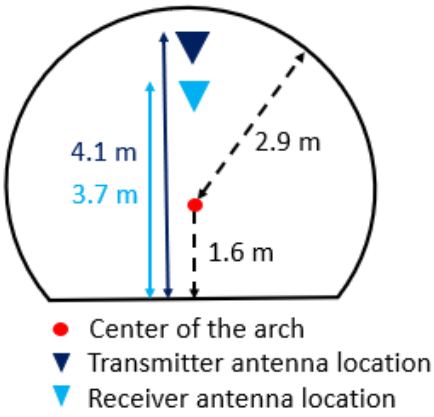

Fig. 1: Dimensions of Tunnel's cross section and antenna locations.

The measured route in tunnels can be categorized into two main segments, a straight segment, and a curved segment. The straight segment under investigation is about 226 m, and after this distance, the tunnel starts curving for 363 m with an ROC of 300 m. The measurement route in the tunnel under investigation is presented in Fig. 2.

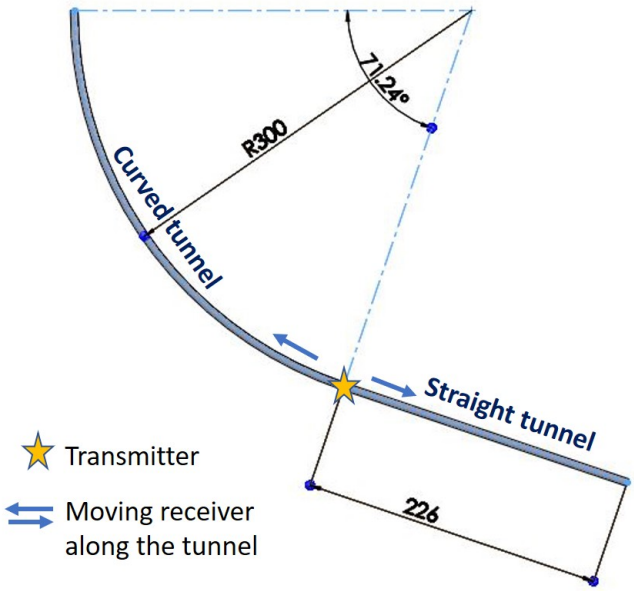

Fig. 2: The measured route in tunnels.

B. Measurement Hardware and Setup

The measurement setup consists of a transmitter and a receiver. At the transmitter side, a signal generator outputs a continuous wave (CW) signal at 2.485 GHz which is radiated through an omnidirectional antenna with a gain of 0 dBi. The transmitted power is fixed at 20 dBm. At the receiver side, a signal analyzer is used to capture the received CW signal from another identical antenna. Through the pre-screening of the environment without channel sounding, a noise floor of -120 dBm is observed at the receiver side. Both the antennas are kept vertically polarized during the measurement campaign and installed on plastic pipes to minimize the radiation pattern distortion. The data logging of the received signal is performed by interfacing the signal analyzer with a laptop using LabView software. The block diagram of measurement configuration and the actual measurement setup on-site is shown in Fig. 3

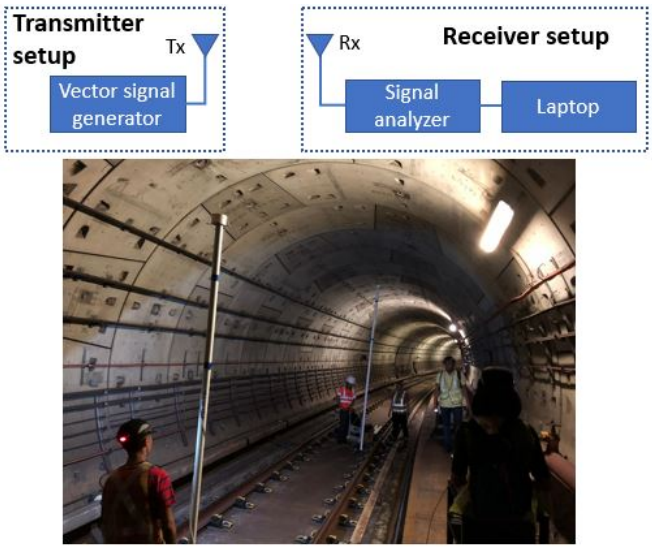

Fig. 3: Measurement configuration with setup on site

C. Measurement Campaign

The main goal of this measurement campaign is to study the radio wave propagation within both the straight and curved tunnels. To achieve this, the transmitter is fixed at a position in-between a straight tunnel and a curved tunnel as shown in Fig. 2. The transmitter antenna is fixed at 4.1 m from the floor of the tunnel. The receiver is moved along the tunnel to capture the propagating characteristics of radio signals. The receiving antenna is placed at 3.7 m from the floor of the tunnel.

It is noted that the height of 3.7 m of the receiving antenna is to simulate the height of the antenna mounted on the train in Singapore. The location of the transmitter and receiver antennas in the tunnel are chosen based on realistic scenarios.

IV. Comparison Study: Straight & Curved Tunnels

In this section, comparative study of measurement results with the simulation results using ray-tracing approach and the calculated results using analytical model (i.e., waveguide model [9] and free space loss (FSL) model [24], [25]) will be performed for the tunnel route as shown in Fig. 2.

A. Benchmark Methods for Comparison

The summarized information of ray tracing approach, waveguide model and FSL model for benchmark comparison can be found below;

1) Ray Tracing Approach: In our work, Wireless Insite software [26] is used to perform the ray-tracing simulations. The tunnel dimensions, measurement route, and related material properties as discussed in the above section are taken into consideration in simulation. In the straight tunnel and curved tunnel scenario, the received power is simulated for every 1 m distance of separation.

2) Waveguide Model: The measurements are performed in an arched tunnel. To use a rectangular waveguide model, the arched tunnel dimensions are mapped to a rectangular tunnel by using the surrogate model [27], [28]. The procedure followed to calculate the corresponding rectangular waveguide dimensions for the arched tunnel are given below.

The width (w) and height (h) of the corresponding rectangular waveguide are calculated as,

$$w = \sqrt{\frac{2s}{1+cos(\theta)}[(\pi-\theta)r_a^2 + h_a^2 tan\theta]}, \tag{2}$$

$$h = \sqrt{\frac{s(1+cos\theta)}{2}[(\pi-\theta)r_a^2 + h_a^2 tan\theta]}, \tag{3}$$

where h_a is the distance from the center of the tunnel to its flat base, r_a is the radius, s and θ are the cross-sectional area ratio of a square model to a circular model which can be calculated through,

$$s = \sqrt[3]{(x_1^o)^4/16\pi)}, \tag{4}$$

$$\theta = \arccos(h_a/r_a), \tag{5}$$

with x_1^o, the first zero of bessels function $J_o(x)$. The calculated w and h values are used in the waveguide model to predict the received power along the tunnel. The predicted received power at any given point (x, y, z) inside the tunnel can be calculated by using the following equation;

$$P_r(x,y,z) = P_t G_t G_r \left(\frac{1}{E_o}\sum_{m=1}^{\infty}\sum_{n=1}^{\infty} C_{mn} E_{m,n}^{eign}(x,y) e^{-(\alpha_{mn}+j\beta_{mn}).z}\right)^2, \tag{6}$$

where E_0 is the field intensity at the transmitter, P_t is the transmitted power, G_t and G_r are the antenna gains of the transmitter and receiver, $E_{m,n}^{eign}$ is the eigen function of field distribution of each mode, $\alpha_{m,n}$ and $\beta_{m,n}$ are the attenuation coefficient and phase-shift coefficient of each mode (m and n indicate wave modes). The mode intensity C_{mn} on the excitation plane is defined as

$$C_{mn} = \frac{4E_o\pi}{wh\sqrt{1-(\frac{m\pi}{wk})^2-(\frac{n\pi}{hk})^2}} sin(\frac{m\pi}{w}x_o+\phi_x)cos(\frac{n\pi}{h}y_o+\phi_y), \tag{7}$$

where k is the wave number which is given as $k = 2\pi f_o\sqrt{\mu_o\epsilon_o\epsilon_a}$. The permeability of vertical/horizontal walls and the air in the tunnel is assumed to be the same and as μ_o. ϵ_o and ϵ_a are the permittivity of free space and the relative permittivity of air in the tunnel. The $E_{m,n}^{eign}$ is the field distribution of each mode in the form of eigen function,

$$E_{m,n}^{eign} \simeq sin(\frac{m\pi}{w}x+\phi_x)cos(\frac{n\pi}{h}y+\phi_y), \tag{8}$$

where $\phi_x = 0$ if m is even and $\phi_x = \pi$ if m is odd, $\phi_y = \pi$ if n is even and $\phi_y = 0$ if n is odd.

The attenuation coefficient α_{mn} and phase coefficient β_{mn} are defined as,

$$\alpha_{mn} = \frac{2}{w}(\frac{m\pi}{wk})^2 Re\frac{\bar{\epsilon_v}}{\sqrt{\bar{\epsilon_v}-1}} + \frac{2}{w}(\frac{n\pi}{hk})^2 Im\frac{1}{\sqrt{\bar{\epsilon_h}-1}}, \tag{9}$$

$$\beta_{mn} = \sqrt{k^2-(\frac{m\pi}{w})^2-(\frac{n\pi}{h})^2}. \tag{10}$$

The $\bar{\epsilon_v} = \epsilon_v + \frac{\sigma_v}{j2\pi f_o\epsilon_o}$ and $\bar{\epsilon_h} = \epsilon_h + \frac{\sigma_h}{j2\pi f_o\epsilon_o}$, where ϵ_v and ϵ_h are the relative permittivity of vertical walls and the horizontal walls of the tunnel. Similarly, the σ_v, σ_h and σ_a are the conductivity of vertical walls, horizontal walls and the air. Here f_o is the center frequency of the signal.

3) FSL Model: The FSL model [24], [25] can be used for determining the signal strength in a free space environment (an ideal case), as presented below

$$L_{FSL} = -27.56 + 20\log_{10}(f) + 20\log_{10}(d), \tag{11}$$

where L_{FSL} is the free space loss in dB, f is the frequency in MHz, and d is the propagation distance in meter.

B. Comparison and Validation of Measurement Results

1) Propagation in Straight Tunnel Route: Fig. 4 presents a comparative study of the measurement results with the simulation results using the ray-tracing approach and the calculated results using the FSL model and the waveguide model for the straight tunnel route. In a tunnel environment, the free space propagation mechanism exists until the first reflected component reaches the receiver antenna according to the Fresnel zone [21]. By considering the location of the transmitter antenna, receiver antenna and the operating frequency of this measurement scenario, at a distance of 12 m (approx.) from the transmitter antenna, the first Fresnel zone touches the tunnel walls [21]. This location is represented using a vertical dashed line in Fig. 4. The region in which the effect of reflected signals is negligible is referred as *the near zone* as discussed in [18]–[22]. In Fig. 4 *the near zone propagation region* is on the left of the vertical dashed line, adjacent to the transmitter antenna. From Fig. 4, it is observed that up to a separation distance of about 12 m from the transmitter, the measured signal strength (large scale) follows the FSL model as well as the ray-tracing simulation.

Radio-wave propagation is influenced by the presence of multi-reflected signals above 12 m (approx.) from the transmitter antenna. The rich multipath phenomena in tunnels can be treated as the multimode propagation of the waveguide model [23]. It is observed that the existence of the waveguiding effect enhances the radio wave propagation in the tunnel, and

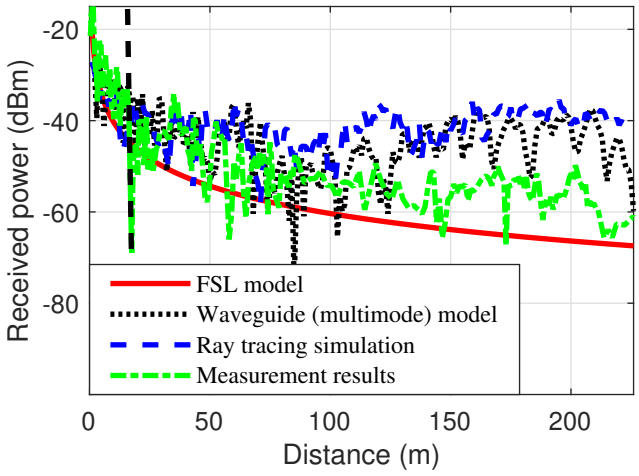

Fig. 4: Comparison and validation of measurement results in straight tunnel, where near zone and far zone are separated by vertical dashed line.

thereby the measured received power exceeds that of free space propagation as shown in Fig. 4. The region in which the effect of multipath propagation shall be considered is referred as *the far zone* [18], [19].

As introduced in literature [6], two different radio wave propagation mechanisms exist in a straight tunnel; *free space propagation mechanism in the near zone*, and *multimode or fundamental mode propagation mechanism in the far zone*. Our measurement results as discussed above further validate the existence of both the propagation mechanisms, which can be observed in Fig. 4 (generally before and after the dashed line). To evaluate the agreement of simulated/calculated results with measured ones, average deviation error, *ADE* as presented in (12) is used [29] ;

$$ADE = \sqrt{\frac{1}{N_z}\sum_{k=1}^{N_z}|P_{simu/calcu} - P_{measured}|^2} \qquad (12)$$

where $P_{simu/calcu}$ and $P_{measured}$ are the simulated/calculated and measured received power, and N_z is the total number of sampling points and 226 for this straight tunnel. From the analysis, the ray-tracing model gives an *ADE* of 13.60 dB when compared to the measurement data. This could be because the simulation parameters in the ray tracing algorithm may deviate from the realistic scenarios, and then cause possible over-consideration of multipath components and their related strength enhancement of radio wave propagation inside the tunnel, and possible misalignment of multipath introduced by constructive/destructive signal summation. It is also noted that the waveguide model developed by Sun and Akyildiz [9], reported better performance with an *ADE* of 11.12 dB.

Additionally, our analysis found that the ray-tracing model gives an ADE of 7.51 dB in the near zone and 12.38 dB in the far zone, while the waveguide model has an ADE of 8.02 dB in the near zone and 11.42 dB in the far zone. Same as those reported in [30] where the ray tracing is found to work better for modeling the complex propagation environment at a shorter distance, the calculated ADE values in this study also suggests that ray tracing can give better performance than the waveguide model in near-zone propagation. The waveguide model is preferred for far-zone channel modeling when compared to the ray tracing approach [21].

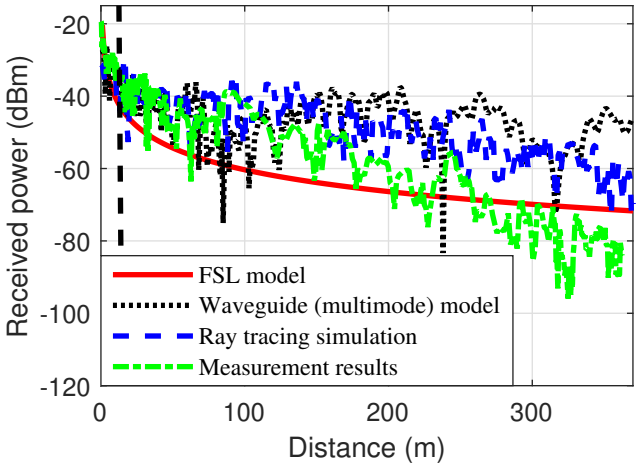

Fig. 5: Comparison and validation of measurement results in curved tunnel, where near zone and far zone are separated by vertical dashed line.

2) Propagation in Curved Tunnel Route: Similar to the comparison results shown in Fig. 4 for the straight tunnel, Fig. 5 presents the results for the curved tunnel route under this investigation. The radio wave propagation in the curved tunnel follows free space propagation firstly until a distance of about 12 m (vertical dashed line) and then is dominated by the waveguiding effect. However, the enhancement of signal strength by the waveguiding effect in the curved tunnel is different from that observed for the straight tunnel. The change in the enhancement of the waveguiding effect can be noticed in curved tunnel ray tracing results and measurement results. To validate the change in waveguiding effect, the curved-tunnel ray tracing and measurement results are compared with FSL and straight-tunnel waveguide model results in Fig. 5.

By this comparison study, we can observe that the change in wave propagation phenomena starts at a distance of about 100 m from the transmitter, where the propagating signal starts to be blocked by tunnel curvature and thereby degrades the received signal strength (even with waveguiding introduced enhancement effect). Through this analysis and observation, it can be concluded that the waveguiding effect in the curved tunnel can be split into *enhanced* waveguiding effect and *degraded* waveguiding effect generally. The *enhanced* waveguiding effect keeps the signal strength higher than that in a free space environment. However, the tunnels curvature could block the rich multipath propagation from farther transmission and then decreases the signal strength much more compared to free space propagation (referred to as *degraded* waveguiding effect).

Similar to the straight-tunnel case, we have also evaluated the ADE of simulated/calculated results with the measurement results. The ray-tracing simulation result has an ADE

of 14.01 dB when compared with measured data. Using the straight-tunnel waveguide model, an ADE error of 18.74 dB is observed when compared with curved-tunnel measurement data. In this evaluation, $N_z = 363$ for the 363 m long curved tunnel.

Similar to the straight tunnel results, the ADE of ray tracing model in the near zone is 3.9 dB which is less than ADE of the waveguide model which is 5 dB. The far zone ADE of the straight tunnel waveguide model is 19 dB which very high compared to the ADE of the ray tracing model (14.23 dB).

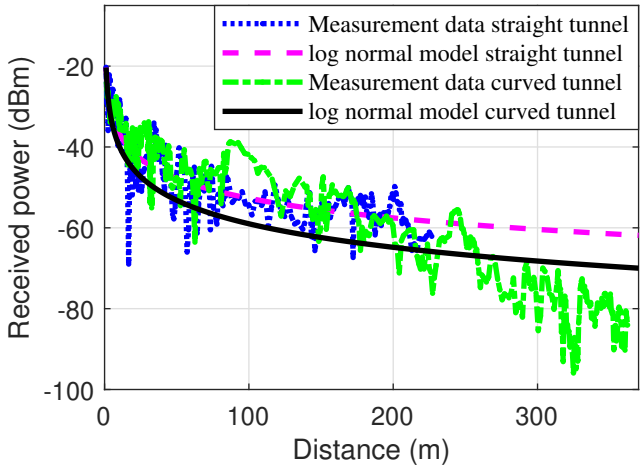

Fig. 6: Measured data with best fitted log-normal models in straight and curved tunnel.

3) Comparison of Straight- and Curved-Tunnel Propagation: Fig. 6 presents the measured received power in both the straight and curved tunnels. Log-normal model as shown in (13) is also used to study their difference, such as the existing of signal blockage due to tunnel curvature in the curved tunnel. The empirical values determined for the parameters of log-normal path loss model in (13), with d_0 = 1 m, are summarized in Table I. It is noted that the log-normal path loss model parameters (n_o, σ) are calculated by performing linear regression onto the measured data, to derive the best fitted curve with a minimum deviation from the raw field data.

$$PL_{LogNorm} = K + 10n_0 \log_{10}(d/d_0) + X_\sigma, \qquad (13)$$

where K is the path loss at a reference distance d_0, n_0 is the path loss exponent (n_0 = 2 for a free space channel), and X_σ is the Gaussian random variable with standard deviation of σ. From Table I, it is found that the path loss exponent $n_0 = 1.93$ in the curved tunnel is higher than that (1.61) in the straight tunnel. This suggests that the signal enhancement is degraded and thereby attenuation rate increases in the curved tunnel. This is highly likely introduced by the tunnel curvature which starts to block the signal after a certain transmission distance.

The σ which represents the signal variation (e.g., caused by shadowing) around the general signal trend in the curved tunnel (9.81 dB) is significantly higher (nearly twice) than that (5.02 dB) in the straight tunnel. This means the shadow fading in the curved tunnel is severe in comparison to the straight tunnel, and a similar observation was also reported in [31]. From Fig. 6, it is also observed that starting from around 100 m in the curved tunnel, the attenuation rate per distance increases as compared to short-distance transmission. The change is due to the appearance of tunnel curvature which starts to block the direct path between the transmitter and the receiver, and then the enhanced waveguiding effect as discussed previously starts to degrade correspondingly. This suggests that the log-normal model with only one attenuation rate (or slope) may not be good enough to represent the radio wave propagation inside the curved tunnel. The location where the direct path is blocked by the tunnel curvature becomes important to predict the signal strength accurately. In the following section, the methodology used to determine the location at which the direct path is blocked by the tunnel curvature and an improved path loss modeling inside the curved tunnel will be discussed.

Tunnel	n_0	σ (dB)
Straight Tunnel	1.61	5.02
Curved Tunnel	1.93	9.81

TABLE I: Empirical values determined for the parameters of log-normal path loss model.

V. Determination of Break Point for Two-slope Path Loss Model

A. Calculation of Break Point

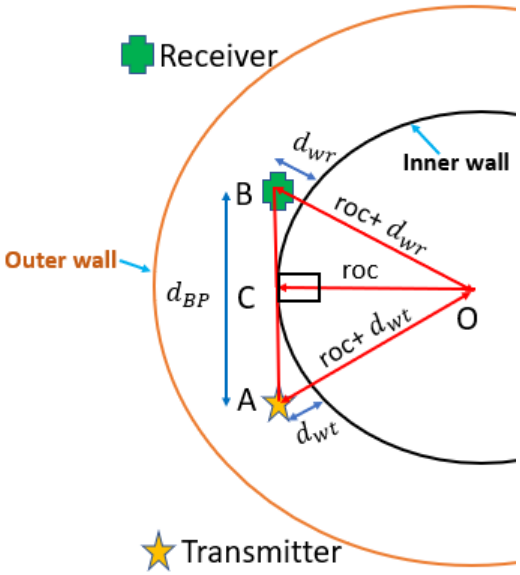

Fig. 7: Graphical representation of the location for break point.

In this study, the distance from the transmitter antenna at which the enhanced radio wave propagation in a curved tunnel starts to be degraded is defined as the *break point*. More specifically, the break point that separates the *enhanced waveguiding mechanism* and the *degraded waveguiding mechanism* in a curved tunnel. The location of the break point can be calculated using the circle and tangent theory for a given ROC

and the transmitter and receiver locations with respect to the tunnel inner wall.

In the following, the determination of break point will be explained using the graphical representation of the location for break point as shown in Fig. 7. Clearly, the distance from tunnel curve origin O to transmitter and receiver is $(roc + d_{wt})$ and $(roc + d_{wr})$, where d_{wt} is the distance between the transmitter and the inner wall of the curved tunnel, d_{wr} is the distance between the receiver and the inner wall of the tunnel, and roc is the radius of curvature. The distance between the transmitter and receiver at which the direct path will touch the tunnel wall at the point C is d_{BP}.

The direct path $\overline{AB}$ is a tangent to the curved tunnel. The line joining the point of tangency C and origin O of the curve is at right angle with the $\overline{AC}$ and $\overline{BC}$. By using this condition, Pythagorean theorem can be applied to calculate d_{BP} which is $\overline{AB}$ here.

$$\overline{AB} = \overline{AC} + \overline{BC} \tag{14}$$

$$\overline{AC} = \sqrt{(roc + d_{wt})^2 - roc^2} \tag{15}$$

$$\overline{BC} = \sqrt{(roc + d_{wr})^2 - roc^2} \tag{16}$$

$$d_{BP} = \overline{AB} = \sqrt{(roc + d_{wt})^2 - roc^2} + \sqrt{(roc + d_{wr})^2 - roc^2} \tag{17}$$

It is clear that the calculated break point will rely on the ROC and the location of the transmitter and receiver within the curved tunnel.

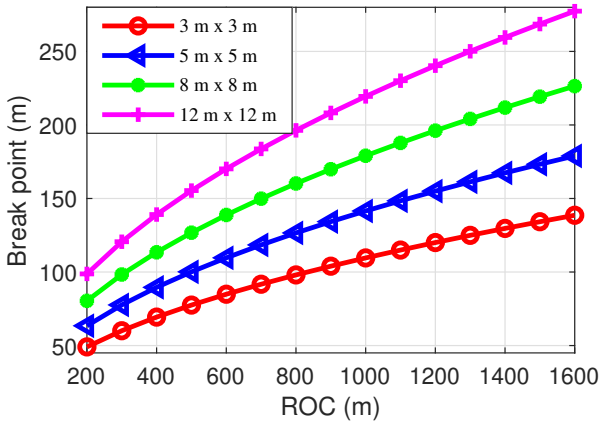

Fig. 8: The relationship between the break point and the ROC.

Fig. 8 shows the relationship between the ROC and the break point for the tunnels of cross-sectional dimensions of $3\ m \times 3\ m$, $5\ m \times 5\ m$, $8\ m \times 8\ m$ and $12\ m \times 12\ m$. The transmitter and receiver are assumed to be at the center of the tunnel in this comparison. From Fig. 8, it can be seen that for a larger ROC, the break point exists at a longer distance. Similarly, for a smaller ROC, the break point exists at a shorter distance. The location of the break point is directly proportional to the ROC. As the dimensions of tunnel increase, the break point will be extended to a farther distance. For a large tunnel dimension with a higher ROC, the effect of curvature can be negligible.

The derived break point can be used to model the curved-tunnel radio wave propagation, to distinguish the *enhanced waveguiding effect* and the *degraded waveguiding effect*. A two-slope path loss model seems to be more suitable to address these two propagation mechanisms, and the break point is the point where a different attenuation rate per distance (i.e., the slope) starts to play its role. Further details and validation of the two-slope path loss model will be discussed in the next subsection.

B. Two-slope Path Loss Model for Curved Tunnel

A two-slope path loss model in (18) is proposed to better model the radio wave propagation in curved tunnel,

$$PL(d) = \begin{cases} K_1 + 10n_1 \log_{10}(d/d_{ref}) + X_{\sigma_1}, & \text{if } d \le d_{BP}; \\ K_2 + 10n_2 \log_{10}(d/d_{BP}) + X_{\sigma_2}, & \text{otherwise.} \end{cases} \tag{18}$$

where K_1 is the free space path loss at a reference distance d_{ref}, K_2 is the free space path loss at d_{BP}, n_1 and n_2 are the path loss exponents, X_{σ_1} and X_{σ_2} are the Gaussian random variables with standard deviation of σ_1 and σ_2. It is noted that this two-slope path loss model could better describe the transition from the *enhanced waveguiding effect* to the *degraded waveguiding effect*, and then offers a more certain path loss for radio planner with a smaller signal variation determined by σ.

1) Empirical Two-slope Model for Curved Tunnel in Singapore with $roc = 300\ m$: With the tunnel dimensions and the antenna locations, the break point for our measurement scenarios in a typical curved tunnel in Singapore is calculated using the proposed method (17). The calculated break point d_{BP} is found to be at around $83\ m$ from the transmitter. With d_{BP}, empirical values for two-slope path loss model (18) were then determined.

Fig. 9 presents the measured data with the best fitted two-slope path loss model with $d_{BP} = 83\ m$ which is shown as a dashed line. From Fig. 9, it is observed that the attenuation rate per distance increases multiple times after the break point. The results also suggest the enriched multipath propagation ($n_1 = 1.16$) in the curved tunnel before the break point. After the break point the dominant multipath components started to be blocked due to the curvature of tunnel. The blockage of tunnel curvature degrades the signal strength, with shadowing introduced ($\sigma_2 = 6.76$ dB which is larger than $\sigma_1 = 4.31$ dB)

2) Empirical Two-slope Model for Curved Tunnel in Spain with roc = 300 m and 500 m: The proposed break point d_{BP} with two-slope path loss model are applied to the measurements results for curved tunnels with $roc = 300\ m$ and $roc = 500\ m$ as reported in [17]. The tunnel investigated in their measurement campaign are arched tunnel ($8.41\ m \times 6.87\ m$). The break point is then calculated by using (17), with the provided locations for their transmitter and receiver.

The measured data with the best fitted two-slope path loss models for the curved tunnels with $roc = 300\ m$ and $roc = 500\ m$ are presented in Fig. 10 and Fig. 11 respectively. It is noted that similar *enhanced waveguiding effect* and

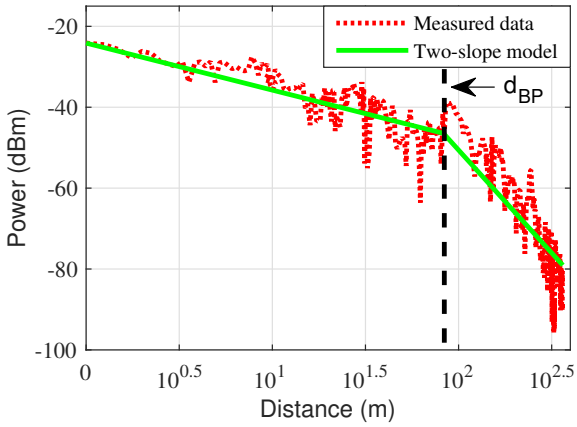

Fig. 9: Measured data vs best fitted two-slope path loss model with $d_{BP} = 83\ m$ for a typical curved tunnel in Singapore, $roc = 300\ m$.

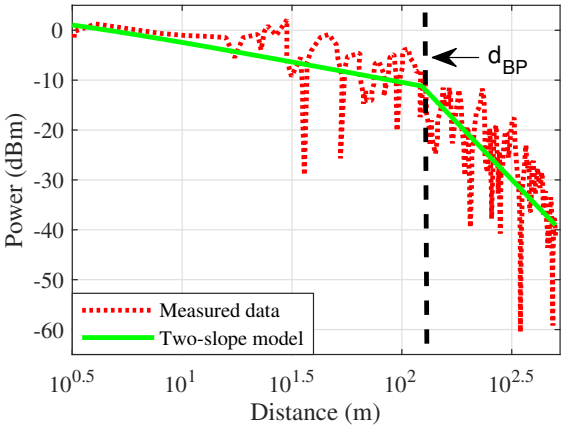

Fig. 11: Measured data vs best fitted two-slope path loss model with $d_{BP} = 124\ m$ for a typical curved tunnel in Spain [17], $roc = 500\ m$.

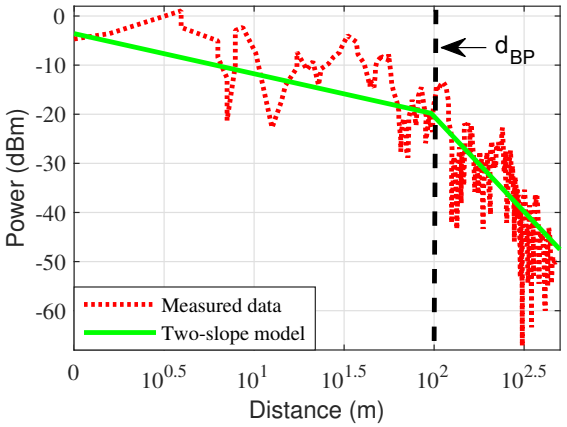

Fig. 10: data vs best fitted two-slope path loss model with $d_{BP} = 96\ m$ for a typical curved tunnel in Spain [17], $roc = 300\ m$.

degraded waveguiding effect due to the blockage from tunnel curvature (before and after the dashed lines which represent the break point locations) are observed, as comparing to the curved tunnel in Singapore. The measurement data shown in Fig. 10 and Fig. 11 is extracted from [17], the data has a sampling interval of around 5 m (approx). Compared to Fig. 9, the lack of adequate number of data samples before the break point might result in degraded fit of the two-slope path loss model.

3) Empirical Two-slope Model for Curved Tunnel in Italy with roc = 780 m: The proposed break point d_{BP} with two-slope path loss model are applied to the data measured from the tunnel with approximately rectangular cross-section ($8.4\ m \times 5.1\ m$) in [12]. The test case B data of curved tunnel with $roc = 780\ m$ is used in this study. The calculated break point is around 217 m from the transmitter, for the reported locations of the antennas. Similar findings as shown in Fig. 9, Fig. 10, and Fig. 11 are observed. It is noted that the lack of sufficient samples of measurement data results in a slightly less fit of the two-slope path loss model in Fig. 12 compared to the results in Fig. 9.

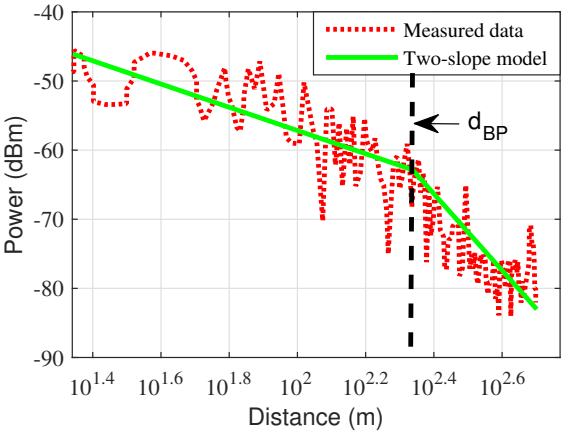

Fig. 12: Measured data vs best fitted two-slope path loss model with $d_{BP} = 217\ m$ for a typical curved tunnel in Italy [12], $roc = 780\ m$.

To have a comparative discussion, empirical values for two-slope path loss model with the proposed break point in different tunnels as presented in Fig. 9 to Fig. 12 are summarised in Table. II. It is noted that, n_1 in all the four cases is far less than 2 which suggests the existence of enhanced waveguiding effect before the break point, and n_2 value ranges from 3.88 to 5.51 which are significantly high due to the degraded waveguiding effect introduced by the blockage/shadowing from the curvature of tunnel. By this comparison table, it can be concluded that the attenuation increases by 3 to 6 times after the break point from the transmitter.

With the similar reason, shadow fading parameter σ_1 before the break point is less than σ_2 after the break point. This is because the shadowing from the curvature of tunnel blocks the

Location	w x h (m)	roc (m)	d_{BP} (m) (approx)	n_1	σ_1 (dB)	ADE_1	n_2	σ_2 (dB)	ADE_2	ADE_c
Singapore	5.8 × 4.5	300	83	1.16	4.31	4.31	5.09	6.76	6.87	6.09
Spain	8.4 × 6.87	300	96	0.82	5.64	5.94	3.88	6.35	6.5	6.37
Spain	8.4 × 6.87	500	124	0.83	5.26	5.3	4.58	6.97	6.9	6.52
Italy	8.4 × 5.1	780	217	1.68	3.96	3.93	5.51	4.42	4.47	4.19

TABLE II: Empirical values for two-slope path loss model with the proposed break point in different tunnels.

strong direct-path signal and weaker multiple-reflected signals reaching the receiver after the break point. Similar findings are also presented in [32].

In addition, the ADE values for the proposed two-slope path loss model are included in Table II as compared to the measurement data. The ADE calculated before the breakpoint (d_{BP}) is represented as ADE_1 and after the breakpoint (d_{BP}) as ADE_2. The ADE for the entire two-slope path loss model is represented as ADE_c. Except for modeling of the curved tunnels in Italy, modeling of all the remaining tunnels presented in Table II results in an ADE_c of about 6 dBm with respect to the two-slope path loss model. The proposed model results in a minimum ADE_1 of 3.93 dB and a maximum ADE_1 of 5.94 dB in modeling the enhanced waveguiding mechanism, and a minimum ADE_2 of 4.47 dB and a maximum ADE_2 of 6.9 dB in modeling the degraded waveguiding mechanism respectively.

VI. Conclusion

In this paper, we reported a recent experimental study to understand the radiowave propagation along a straight tunnel and a curved tunnel at 2.4 GHz. Ray tracing results and waveguide model have been used for comparison with the measurement results. It is found that simulation results have low accuracy due to the limited (or less accurate) site information available. This study also indicated that the curved tunnel has an enriched waveguiding effect which is similar to that in the straight tunnel, before the direct path is being blocked by the tunnel curvature. The waveguiding effect will be degraded once the tunnel curvature starts blocking the direct path.

Our investigation shows that this phenomenon can be well-modeled by introducing the concept of "break point", which can be determined using circle and tangent theory with the ROC of the tunnel and the distance of the transmitter and the receiver from the tunnel wall. It is found that two-slope path loss model could better describe the transition from the *enhanced waveguiding effect* to the *degraded waveguiding effect* in curved tunnels with the calculated break point, and then offers a more certain path loss for radio planner. The proposed methodology in calculating curved-tunnel path loss was applied onto different tunnels with the ROC of 300 m, 500 m and 780 m. The results suggested that the attenuation rate in the curved tunnels can increase by 3 to 6 times after the break point.

Acknowledgment

This research work was conducted in the SMRT-NTU Smart Urban Rail Corporate Laboratory with funding support from the National Research Foundation (NRF), SMRT and Nanyang Technological University; under the Corp Lab@University Scheme. The authors would like to thank Wong Loke Loong, Kevin Kho, Jake Ong Hock Chye, Desmond Kho Kay Leng and Dr. Shilpa Manandhar for their support in performing the channel measurements.

References

[1] J. Farooq and J. Soler, "Radio communication for communications-based train control (cbtc): A tutorial and survey," *IEEE Communications Surveys & Tutorials*, vol. 19, no. 3, pp. 1377–1402, 2017.

[2] M. Fitzmaurice, "Wayside communications: Cbtc data communications subsystems," *IEEE Vehicular Technology Magazine*, vol. 8, no. 3, pp. 73–80, 2013.

[3] S. Fathi-Kazerooni, Y. Kaymak, R. Rojas-Cessa, J. Feng, N. Ansari, M. Zhou, and T. Zhang, "Optimal positioning of ground base stations in free-space optical communications for high-speed trains," *IEEE Transactions on Intelligent Transportation Systems*, vol. 19, no. 6, pp. 1940–1949, 2017.

[4] M. Taheri, N. Ansari, J. Feng, R. Rojas-Cessa, and M. Zhou, "Provisioning internet access using fso in high-speed rail networks," *IEEE Network*, vol. 31, no. 4, pp. 96–101, 2017.

[5] A. Aziminejad, A. W. Lee, and G. Epelbaum, "Underground communication: Radio propagation prediction for cbtc data communication subsystem design," *IEEE Vehicular Technology Magazine*, vol. 10, no. 3, pp. 71–79, 2015.

[6] A. Hrovat, G. Kandus, and T. Javornik, "A survey of radio propagation modeling for tunnels," *IEEE Communications Surveys & Tutorials*, vol. 16, no. 2, pp. 658–669, 2013.

[7] M. D. Bedford, G. A. Kennedy, and P. J. Foster, "Radio transmission characteristics in tunnel environments," *Mining Technology*, vol. 126, no. 2, pp. 77–87, 2017.

[8] S. F. Mahmoud and J. R. Wait, "Guided electromagnetic waves in a curved rectangular mine tunnel," *Radio Science*, vol. 9, no. 5, pp. 567–572, 1974.

[9] Z. Sun and I. F. Akyildiz, "Channel modeling and analysis for wireless networks in underground mines and road tunnels," *IEEE Transactions on communications*, vol. 58, no. 6, 2010.

[10] J. S. Lamminmäki and J. J. Lempiäinen, "Radio propagation characteristics in curved tunnels," *IEE Proceedings-Microwaves, Antennas and Propagation*, vol. 145, no. 4, pp. 327–331, 1998.

[11] D. Didascalou, M. Dottling, T. Zwick, and W. Wiesbeck, "A novel ray-optical approach to model wave propagation in curved tunnels," in *Gateway to 21st Century Communications Village. VTC 1999-Fall. IEEE VTS 50th Vehicular Technology Conference (Cat. No. 99CH36324)*, vol. 4. IEEE, 1999, pp. 2313–2317.

[12] F. Fuschini and G. Falciasecca, "A mixed rays−Modes approach to the propagation in real road and railway tunnels," *IEEE Transactions on Antennas and Propagation*, vol. 60, no. 2, pp. 1095–1105, 2011.

[13] K. Guan, B. Ai, Z. Zhong, C. F. López, L. Zhang, C. Briso-Rodríguez, A. Hrovat, B. Zhang, R. He, and T. Tang, "Measurements and analysis of large-scale fading characteristics in curved subway tunnels at 920 mhz, 2400 mhz, and 5705 mhz," *IEEE Transactions on Intelligent Transportation Systems*, vol. 16, no. 5, pp. 2393–2405, 2015.

[14] Y. Huo, Z. Xu, H.-d. Zheng, and X. Zhou, "Effect of antenna on propagation characteristics of electromagnetic waves in tunnel environments," in *Microelectronics & Electronics, 2009. PrimeAsia 2009. Asia Pacific Conference on Postgraduate Research in*. IEEE, 2009, pp. 268–271.

[15] L. Cheng, L. Zhang, and J. Li, "Influence of mine tunnel wall humidity on electromagnetic waves propagation," *International Journal of Antennas and Propagation*, vol. 2012, 2012.

[16] J. Sun, L. Cheng, and X. Liu, "Influence of electrical parameters on uhf radio propagation in tunnels," in *2004 Joint Conference of the 10th Asia-Pacific Conference on Communications and the 5th International Symposium on Multi-Dimensional Mobile Communications Proceeding*, vol. 1, Aug.-Sept. 2004, pp. 436–438.

[17] B. Ai, K. Guan, Z. Zhong, C. F. López, L. Zhang, C. Briso-Rodriguez, and R. He, "Measurement and analysis of extra propagation loss of tunnel curve," *IEEE Transactions on Vehicular Technology*, vol. 65, no. 4, pp. 1847–1858, 2015.

[18] Y. Zhang and Y. Hwang, "Enhancement of rectangular tunnel waveguide model," in *Proceedings of 1997 Asia-Pacific Microwave Conference*, vol. 1, 1997, pp. 197–200.

[19] Y. P. Zhang, "Novel model for propagation loss prediction in tunnels," *IEEE Transactions on Vehicular Technology*, vol. 52, no. 5, pp. 1308–1314, 2003.

[20] A. Hrovat, G. Kandus, and T. Javornik, "Four-slope channel model for path loss prediction in tunnels at 400 mhz," *IET Microwaves, Antennas & Propagation*, vol. 4, no. 5, pp. 571–582, 2010.

[21] K. Guan, Z. Zhong, B. Ai, R. He, B. Chen, Y. Li, and C. Briso-Rodriguez, "Complete propagation model in tunnels," *IEEE Antennas and Wireless Propagation Letters*, vol. 12, pp. 741–744, 2013.

[22] A. Hrovat and T. Javornik, "Analysis of radio propagation models for smart city applications," *Int. J. Commun*, vol. 7, no. 4, pp. 83–92, 2013.

[23] K. Guan, Z. Zhong, B. Ai, R. He, and C. Briso-Rodriguez, "Five-zone propagation model for large-size vehicles inside tunnels," *Progress In Electromagnetics Research*, vol. 138, pp. 389–405, 2013.

[24] J. D. Parsons, *The Mobile Radio Propagation Channel*. 2nd ed., Wiley, 2000.

[25] Y. H. Lee, F. Dong, and Y. S. Meng, "Near sea-surface mobile radiowave propagation at 5 ghz: Measurements and modeling," *Radioengineering*, vol. 23, no. 3, pp. 824–830, Sept. 2014.

[26] REMCOM, "Wireless insite." [Online]. Available: https://www.remcom.com/wireless-insite-em-propagation-software

[27] S. F. Mahmoud, "Wireless transmission in tunnels with non-circular cross section," *IEEE Transactions on Antennas and Propagation*, vol. 58, no. 2, pp. 613–616, 2009.

[28] X. Zhang, N. Sood, and C. D. Sarris, "Fast radio-wave propagation modeling in tunnels with a hybrid vector parabolic equation/waveguide mode theory method," *IEEE Transactions on Antennas and Propagation*, vol. 66, no. 12, pp. 6540–6551, 2018.

[29] X. Zhang and C. D. Sarris, "Vector parabolic equation-based derivation of rectangular waveguide surrogate models of arched tunnels," *IEEE Transactions on Antennas and Propagation*, vol. 66, no. 3, pp. 1392–1403, 2017.

[30] X. Zhang, N. Sood, J. K. Siu, and C. D. Sarris, "A hybrid ray-tracing/vector parabolic equation method for propagation modeling in train communication channels," *IEEE Transactions on Antennas and Propagation*, vol. 64, no. 5, pp. 1840–1849, 2016.

[31] C. Briso-Rodríguez, J. M. Cruz, and J. I. Alonso, "Measurements and modeling of distributed antenna systems in railway tunnels," *IEEE Transactions on Vehicular Technology*, vol. 56, no. 5, pp. 2870–2879, 2007.

[32] K. Guan, Z. Zhong, J. I. Alonso, and C. Briso-Rodríguez, "Measurement of distributed antenna systems at 2.4 ghz in a realistic subway tunnel environment," *IEEE Transactions on Vehicular Technology*, vol. 61, no. 2, pp. 834–837, 2011.

Kalyankar Shravan Kumar received his B.Tech degree from Jawaharlal Nehru Technological University Hyderabad (JNTUH), Inda in 2014 and M. Tech degree from Indian Institute of Technology Gandhinagar, Inda in 2017. He is currently pursuing the Ph.D. degree with the School of Electrical and Electronic Engineering, Nanyang Technological University, Singapore. His research interests include the channel modeling for indoor environments, subway tunnels and sea to land propagation.

Yee Hui Lee (($S'96^{\smile}M'02^{\smile}SM'11$)) received the B.Eng. (Hons.) and M.Eng. degrees from the School of Electrical and Electronics Engineering, Nanyang Technological University, Singapore, in 1996 and 1998, respectively, and the Ph.D. degree from the University of York, York, U.K., in 2002. Since 2002, she has been a Faculty Member with anyang Technological University, where she is currently an Associate Professor with the School of Electrical and Electronic Engineering. Her research interests include the channel characterization, rain propagation, antenna design, electromagnetic bandgap structures, and evolutionary techniques.

Yu Song Meng (*S* 09 11) received the B.Eng. (Hons.) and Ph.D. degrees in electrical and electronic engineering from Nanyang Technological University, Singapore, in 2005 and 2010 respectively.

He was a Research Engineer with the School of Electrical and Electronic Engineering, Nanyang Technological University, from 2008 to 2009. He joined the Institute for Infocomm Research, Agency for Science, Technology and Research (A*STAR), Singapore, in 2009 as a Research Fellow and then a Scientist I. In 2011, he was transferred to the National Metrology Centre, A*STAR, where he is currently appointed as a Senior Scientist I. From 2012 to 2014, he was part-timely seconded to Psiber Data Pte. Ltd., Singapore, where he was involved in metrological development and assurance of a handheld cable analyser, under a national Technology for Enterprise Capability Upgrading (T-Up) scheme of Singapore. Concurrently, he also serves as a Technical Assessor for the Singapore Accreditation Council – Singapore Laboratory Accreditation Scheme (SAC-SINGLAS) in the field of RF and microwave metrology. His current research interests include electromagnetic metrology, electromagnetic measurements and standards, and electromagnetic-wave propagations.

Dr. Meng is a member of the IEEE Microwave Theory and Techniques Society. He is a recipient of the Asia Pacific Metrology Programme (APMP) Iizuka Young Metrologist Award in 2017 and the national T-Up Excellence Award in 2015.